Theoretical Foundation of the Relationship between Three Definitions of Effective Density and Particle Size

Long Peng [1,2,3,4,*] and Yonglin Liu [1,2,3,5]

1   Institute for Environmental and Climate Research, Jinan University, Guangzhou 511443, China; yonglin102@gmail.com
2   State Key Laboratory Organic Geochemistry, Guangzhou Institute of Geochemistry, Chinese Academy of Sciences, Guangzhou 510640, China
3   Guangdong Provincial Key Laboratory of Environmental Protection and Resources Utilization, Chinese Academy of Sciences, Guangzhou 510640, China
4   Department of Chemistry, University of British Columbia, Vancouver, BC V6T 1Z1, Canada
5   Hangzhou Puyu Technology Development Co., Ltd., Hangzhou 311305, China
*   Correspondence: penglong@jnu.edu.cn

Abstract: Effective density (ρ_e) is universally used in atmospheric science as an alternative measure of the density (ρ) of aerosol particles, and its definitions can be expressed in terms of the particle mass (m_p), ρ, mobility diameter (D_m), vacuum aerodynamic diameter (D_{va}), and dynamic shape factor (χ), as $\rho_e^I = 6m_p/(\pi \cdot D_m^3)$, $\rho_e^{II} = \rho/\chi$, and $\rho_e^{III} = D_{va}/D_m$. However, the theoretical foundation of these three definitions of ρ_e is still poorly understood before their application. Here, we explore the relationship between ρ_e and aerosol size through theoretical calculation. This study finds, for the first time, that ρ_e^I and ρ_e^{III} inherently decrease with increasing size for aspherical particles with a fixed ρ and χ. We further elucidate that these inherent decreasing tendencies are governed by χ, and the ratio of the Cunningham Slip Correction Factor of the volume-equivalent diameter to that of the mobility diameter ($C_c(D_{ve})/C_c(D_m)$), but not by ρ. Taking the variable χ into consideration, the relationships of ρ_e^I and ρ_e^{III} to particle size become more complicated, which suggests that the values of ρ_e^I and ρ_e^{III} have little indication of the size-resolved physicochemical properties of particles. On the contrary, ρ_e^{II} is independent on size for fixed χ and ρ, which indicates that the change in ρ_e^{II} with size can better indicate the change in morphology and the transformation of the chemical compositions of particles. Our new insights into the essence of three ρ_es provide an accurate and crucial theoretical foundation for their application.

Keywords: effective density; dynamic shape factor; chemical composition; size

1. Introduction

Atmospheric particles play an important role in air quality, human health, and global climate change, which strongly depend on their chemical and physical properties [1,2]. Effective density (ρ_e), one of the physical quantities, has been widely adopted in the characterization of the properties of aerosols as an alternative measure of density (ρ) [3,4]. ρ_e can serve as a link between the important characteristics of aerosol particles, such as volume-equivalent diameter (D_{ve}) and aerodynamic diameter (D_a) (presented in Appendix A—Table A1) [5], and as a tracer for new particle formation [6,7] and the atmospheric ageing processes [8]. Moreover, ρ_e can also provide an insight into particle morphology [9].

Due to differences in measurement methods, three effective densities are defined in atmospheric science, which are systematically reviewed in the work of DeCarlo, et al. [10]. The first definition (ρ_e^I) describes ρ_e as the ratio of the particle mass (m_p) to the apparent

volume, calculated assuming a spherical particle with a diameter equal to the measured mobility diameter (D_m) (presented in Appendix A—Table A1) [10]:

$$\rho_e^I = \frac{6m_p}{\pi {D_m}^3} \tag{1}$$

where m_p is equal to $1/6\,\pi \cdot \rho \cdot {D_{ve}}^3$. D_m is related to D_{ve}, as shown in Equation (2):

$$\frac{D_m}{C_c(D_m)} = \frac{D_{ve}}{C_c(D_{ve})} \chi \tag{2}$$

where χ is the dynamic shape factor and $C_c(D)$ represents the Cunningham Slip Correction Factor, which is calculated by Equation (3):

$$C_c(D) = 1 + \frac{\lambda}{D}\left(A + B \cdot \exp\left(\frac{C \cdot D}{\lambda}\right)\right) \tag{3}$$

where λ is the mean free path of the gas molecules, and A, B and C are empirically determined constants specific to the analysis system. Substituting Equation (2) into Equation (1) results in the final form of ρ_e^I, as shown in Equation (4):

$$\rho_e^I = \frac{\rho}{\chi^3} \cdot \left(\frac{C_c(D_{ve})}{C_c(D_m)}\right)^3 \tag{4}$$

The second definition (ρ_e^{II}) is the ratio of ρ to χ [11]:

$$\rho_e^{II} = \frac{\rho}{\chi} \tag{5}$$

The third definition (ρ_e^{III}) is the ratio of vacuum aerodynamic diameter (D_{va}) (presented in Appendix A) and D_m:

$$\rho_e^{III} = \frac{D_{va}}{D_m}\rho_0 \tag{6}$$

where ρ_0 represents the standard density of 1.0 g/cm^3 [10]. D_{va} also depends on D_{ve}:

$$D_{va} = \frac{\rho}{\rho_0}\frac{D_{ve}}{\chi} \tag{7}$$

Combining the Equations (2), (6), and (7) obtains the final form of ρ_e^{III}, as shown in Equation (8) [12].

$$\rho_e^{III} = \frac{C_c(D_{ve})}{\chi^2 \cdot C_c(D_m)}\rho \tag{8}$$

For spherical particles, three ρ_es are equal to their ρ. For aspherical particles, the three definitions of ρ_e should not yield the same numerical values, because they capture slightly different particle properties [10].

Based on the three definitions of effective density, copious studies have measured the values of aerosol effective density using different methods [13]. Hitherto, ρ_e^I is the most widely used definition in atmospheric science, because it can be measured using a variety of simple methods [13], such as the setup of a differential mobility analyzer (DMA), centrifugal particle mass analyzer (CPMA), condensation particle counter (CPC) [14], and DMA single-particle soot photometer (SP2) [15]. Although ρ_e^{III} can be measured using the tandem setup of a DMA—mass spectrometer [16] and the parallel setup of a scanning mobility particle spectrometer (SMPS) and aerosol mass spectrometer (AMS) [17], there are not many studies using the values of this definition to characterize aerosol properties [18–20]. Worse than ρ_e^{III}, until recently, there was no method to measure the value of ρ_e^{II} of an aspherical particle. However, Peng et al. filled this gap by developing a new method

of combining an aerodynamic aerosol classifier (AAC) with single-particle aerosol mass spectrometry (SPAMS) [21]. By using the established methods, previous studies measured the size-resolved ρ_e to indicate the change in morphology and/or the transformation of the chemical compositions of particles. Some studies reported ρ_e decreasing with an increase in particle size [22–27], while the other studies found ρ_e to be independent of [28] or to increase [7] with particle size. These studies ascribed such discrepancies among the particles with different sizes to different voids [24,26], χ [23,25], morphology [4], chemical composition [8], and/or atmospheric processes [29,30]. However, the inherent relationship between the three definitions of ρ_e and the particle size were not understood before their application in these studies.

In this study, we focus on the theoretical calculation of ρ_e to probe the inherent relationship between ρ_e and the particle size for the three definitions of ρ_e, and to explore the factors resulting in their inherent relationship.

2. Materials and Methods

Table 1 presents the set values of ρ, χ, and D_m for Y and Z particles, which were used as surrogate particles in this study. ρ_e^{I}, ρ_e^{II} and ρ_e^{III} for these particles, with a D_m of 40 nm, 80 nm, 150 nm, 250 nm, 350 nm, 450 nm, and 550 nm, were calculated using the values of ρ, χ, and $C_c(D)$. Although Zieger, et al. [31] found that the χ of NaCl depends on particle size, which suggests that χ varies with particle size, we first assumed particles with a fixed χ value in the calculation, to facilitate probing the essential relationship between the three ρ_es and particle size. In this study, the effect of variable χ on the relationship between ρ_e and size is discussed.

Table 1. Information (ρ, χ, and D_m) for calculating the three ρ_e for particles of Y and Z.

| Particles	ρ (g/cm^3)	χ	D_m (nm)
Y	1.0 1.4 1.8 2.2 2.6 3.0 3.4	2.00	
Z	1.80	1.05 1.10 1.20 1.60 2.00 2.50	40, 80, 150, 250, 350, 450, and 550

3. Results and Discussions

3.1. The Decrease in ρ_e^{I} and ρ_e^{III} with Particle Size for Aspherical Particles

Figure 1a,b presents the values of ρ_e^{I} and ρ_e^{III} for the Y and Z particles, respectively, which show that ρ_e^{I} and ρ_e^{III} decrease as the size increases for aspherical particles with fixed ρ and χ. This result highlights, for the first time, the correlation of ρ_e^{I} and ρ_e^{III} with particle size through theoretical analysis. However, the inherent dependency of ρ_e^{I} and ρ_e^{III} on particle size was not considered in previous studies [17,20,32–36]. This omission raises concerns regarding the measurement technologies for ρ_e^{I} and ρ_e^{III} and the results of the morphology, voids, and atmospheric processes of the particles.

We take a closer look at the studies that adopted ρ_e^{I} and ρ_e^{III}. Previous studies established the methods of ρ_e^{I} through the measurement of D_m and D_a, and of ρ_e^{III} through the measurement of D_m and D_{va}. ρ_e^{I} and ρ_e^{III} were determined by fitting the size distributions of D_m and D_a in a narrow-overlap size range [32–35] or using the peak diameters of D_m and D_{va} [17,20], respectively. If the studies applied these methods to measure the size distributions of the particles with a ρ of 1.8 g/cm^3 and a χ of 2.5, it would result in one value

to characterize ρ_e^I and ρ_e^{III}. However, this is inconsistent with the theoretical calculation in this study, which finds that the effective density of these particles ranges from 0.43 g/cm^3 at 40 nm to 0.22 g/cm^3 at 550 nm for ρ_e^I, and from 0.45 g/cm^3 at 40 nm to 0.36 g/cm^3 at 550 nm for ρ_e^{III}, respectively (Figure 1b). This suggests that using specific values for ρ_e^I and ρ_e^{III} to represent the whole measured size range needs to be reevaluated in future studies.
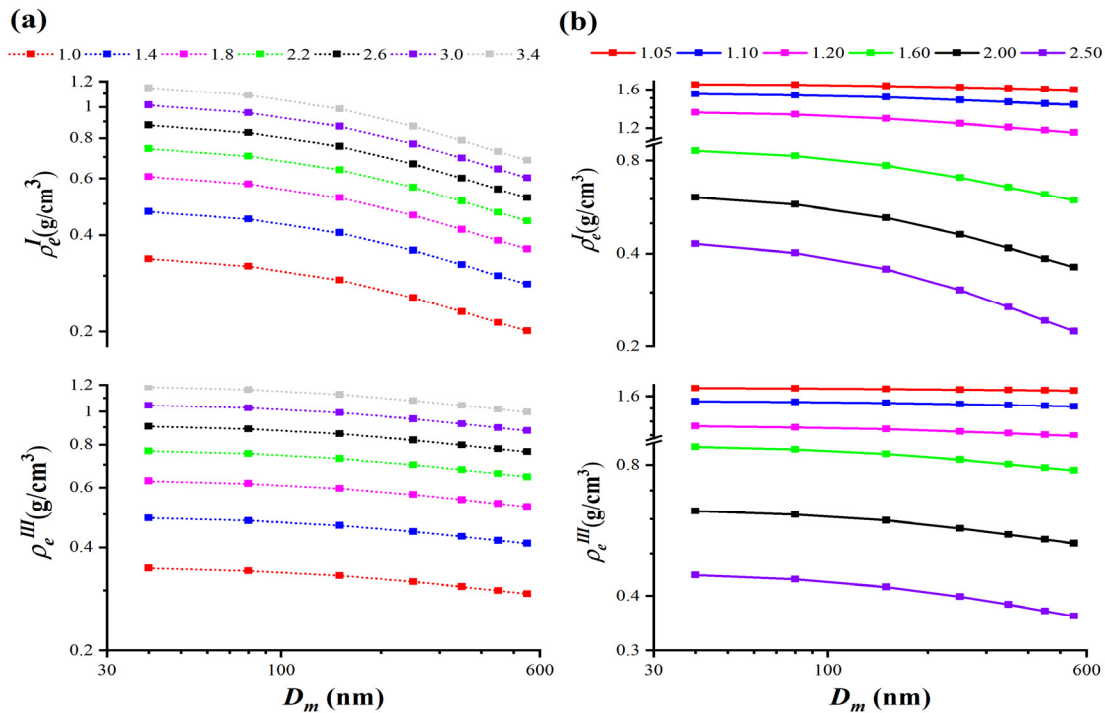
Figure 1. (**a**) The size variations of ρ_e^I and ρ_e^{III} for the Y particles. The change in color from red to grey represents the increase in density from 1.0 to 3.4 g/cm^3; (**b**) The size variations of ρ_e^I and ρ_e^{III} for the Z particles. The change in color from red to purple represents the increase in dynamic shape factor from 1.05 to 2.50.

Park, et al. [22] found, for the first time, that the ρ_e^I of diesel particles decreases as particle size increases. Since then, dozens of studies have shown that the ρ_e^I and ρ_e^{III} of the primary particles, such as particles from vehicles [36,37] and biomass burning [19,38–40], exhibited a similar trend with particle size. These studies attributed this phenomenon to the increasing χ [23,25] and more voids [24,26] with a large D_m. However, we obtained the size-resolved ρ_e^I and ρ_e^{III} for soot with fixed χ and found that the effective density still decreases with the increasing particle size, even without the increase in the voids. Therefore, it is somewhat arbitrary to conclude that larger particles have a larger χ and more voids based only on the measurements of ρ_e^I and ρ_e^{III} with different particle sizes.

The values of ρ_e^I and ρ_e^{III} are generally used to indicate the aging process of particles in the atmosphere [8,41–43]. The atmospheric aging processes would change the size of the particles and, consequently, influence ρ_e^I and ρ_e^{III}, based on our theoretical calculation. Therefore, the change in ρ_e^I and ρ_e^{III} due to aging processes might be biased if the essence of ρ_e^I and ρ_e^{III} with particle size is not considered.

3.2. The Factors That Cause the Decrease in ρ_e^I and ρ_e^{III} with Particle Size

According to Equations (4) and (8), ρ_e^I and ρ_e^{III} are a function of ρ, χ, and $C_c(D_{ve})/C_c(D_m)$, so the three factors were evaluated for the decrease in ρ_e^I and ρ_e^{III} with particle size. ρ was evaluated by Y particles with fixed χ but with the variable ρ. Figure 1a shows the variations of ρ_e^I and ρ_e^{III} of the Y particles. The values of ρ_e^I and ρ_e^{III} decrease monotonically with D_m, and ρ_e^I decreases more rapidly than ρ_e^{III}. Correspondingly, Figure 2a shows the $\Delta\rho$ ($\rho_{e,40nm} - \rho_{e,550nm}$) and R (($\rho_{e,40nm} - \rho_{e,550nm}$)/$\rho_{e,550nm}$) of ρ_e^I and ρ_e^{III} of the Y particles as

a function of ρ. Obviously, $\Delta\rho$ is proportional to ρ and the slope of $\rho_e{}^I$ is greater than that of $\rho_e{}^{III}$, which is a result of the larger coefficient between $\rho_e{}^I$ and ρ $((C_c(D_{ve})/C_c(D_m))^3/\chi^3)$ (as shown in Equation (4)) than between $\rho_e{}^{III}$ and ρ $(C_c(D_{ve})/C_c(D_m)/\chi^2)$ (as shown in Equation (8)). In particular, $\rho_e{}^I$ and $\rho_e{}^{III}$ have constant R $((\rho_{e,40\text{nm}} - \rho_{e,550\text{nm}})/\rho_{e,550\text{nm}})$ values of 68.0% and 18.9%, respectively. These findings lead to the conclusion that ρ determines the values of $\rho_e{}^I$ and $\rho_e{}^{III}$, but does not affect the relationship of $\rho_e{}^I$ and $\rho_e{}^{III}$ with the particle size.
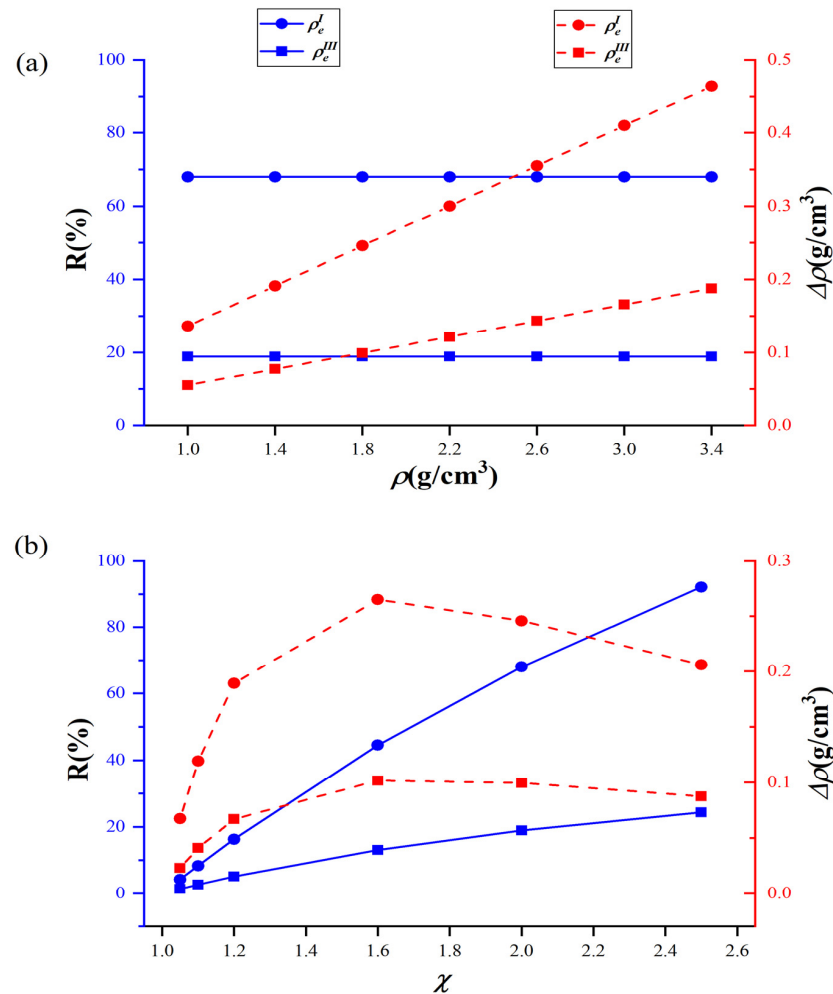

Figure 2. (a) $\Delta\rho$ $(=\rho_{e,40\text{nm}} - \rho_{e,550\text{nm}})$ and R $(=\Delta\rho/\rho_{e,550\text{nm}})$ of $\rho_e{}^I$ and $\rho_e{}^{III}$ for the Y particles with different ρ; (b) $\Delta\rho$ $(=\rho_{e,40\text{nm}} - \rho_{e,550\text{nm}})$ and R $(=\Delta\rho/\rho_{e,550\text{nm}})$ of $\rho_e{}^I$ and $\rho_e{}^{III}$ for the Z particles with different χ. Red and blue lines represent $\Delta\rho$ and R, respectively.

To explore the effects of χ on the decrease in $\rho_e{}^I$ and $\rho_e{}^{III}$ with particle size, the $\rho_e{}^I$ and $\rho_e{}^{III}$ of the series of Z particles with a fixed ρ but the variable χ are calculated and presented in Figure 1b. For particles with one value of D_m, $\rho_e{}^I$ and $\rho_e{}^{III}$ decrease with increasing χ. For $\chi > 1.00$, $\rho_e{}^I$ and $\rho_e{}^{III}$ decrease with increasing D_m. Figure 2b shows $\Delta\rho$ $(\rho_{e,40\text{nm}} - \rho_{e,550\text{nm}})$ and R $(\Delta\rho/\rho_{e,550\text{nm}})$ of $\rho_e{}^I$ and $\rho_e{}^{III}$ of the Z particles. $\Delta\rho$ increases from 0.07 to 0.26 g/cm^3 for $\rho_e{}^I$ and from 0.02 to 0.10 g/cm^3 for $\rho_e{}^{III}$, as χ increases from 1.05 to 1.60. Then, $\Delta\rho$ decreases from 0.26 g/cm^3 to 0.21 g/cm^3 for $\rho_e{}^I$ and from 0.10 g/cm^3 to 0.09 g/cm^3 for $\rho_e{}^{III}$, as χ increases from 1.60 to 2.50. Additionally, R increases from 4.2% to 92.1% for $\rho_e{}^I$, and increases from 1.4% to 24.3% for $\rho_e{}^{III}$, as χ increases from 1.05 to 2.50. This implies that χ plays a key role in the values of $\rho_e{}^I$ and $\rho_e{}^{III}$ and their dependence on particle size.

$\rho_e{}^I$ and $\rho_e{}^{III}$ for the aspherical particles with fixed ρ and χ, however, still depend on D_m, suggesting that $C_c(D_{ve})/C_c(D_m)$ is responsible for the dependency. Figure 3 shows the relationship between $C_c(D_{ve})/C_c(D_m)$ and particle size for the Z particles with a ρ of

1.80 g/cm^3 and a χ ranging from 1.05 to 2.50. It can be seen that $C_c(D_{ve})/C_c(D_m)$ is greater than 1 in the size range of 40–550 nm, and decreases slightly from 1.02 to 1.01 (0.9%), 1.05 to 1.02 (2.9%), and 1.09 to 1.04 (4.8%) for the particles with a χ of 1.05, 1.10, and 1.20, respectively. The values of $C_c(D_{ve})/C_c(D_m)$ have an evident downward trend, decreasing from 1.25 to 1.11 (12.6%), 1.39 to 1.17 (18.8%), and 1.55 to 1.25 (24.0%) for the particles with a χ of 1.60, 2.00 and 2.50, respectively. Obviously, when χ is larger, $C_c(D_{ve})/C_c(D_m)$ decreases more rapidly with D_m.
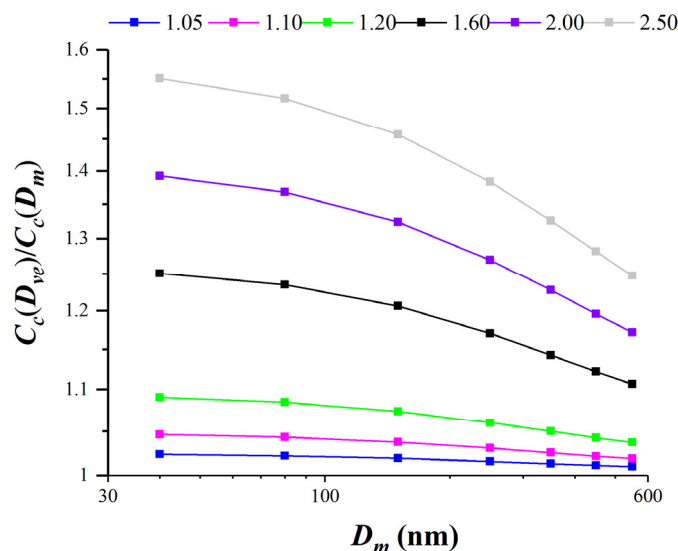
Figure 3. The relationship between the $C_c(D_{ve})/C_c(D_m)$ and D_m for the Z particles with fixed ρ of 1.80 g/cm^3 and different χ values of 1.05, 1.10,1.20, 1.60, 2.00, and 2.50, which are represented by different colors.

In this study, through the exploitation of the final forms of ρ_e^I and ρ_e^{III} (i.e., Equations (4) and (8)), we discover that ρ_e^I is proportional to $(C_c(D_{ve})/C_c(D_m))^3$, and ρ_e^{III} is proportional to $C_c(D_{ve})/C_c(D_m)$. $C_c(D_{ve})/C_c(D_m)$ decreases as D_m increases (Figure 3), and therefore, ρ_e^I and ρ_e^{III} also definitely decrease as D_m increases. The role of χ on $C_c(D_{ve})/C_c(D_m)$ also explains why χ determines the downward trends of ρ_e^I and ρ_e^{III} (Figure 2b). Furthermore, the cube value of $C_c(D_{ve})/C_c(D_m)$ is greater than itself because it is greater than 1, which inevitably causes a faster downward trend of ρ_e^I with D_m than that of ρ_e^{III}. Generally, the values of χ and $C_c(D_{ve})$ are unknown when using effective density to substitute for density; therefore, the downward trends of ρ_e^I and ρ_e^{III} cannot be corrected in their application.

ρ_e^I and ρ_e^{III} inherently decrease with the increasing size of aspherical particles, indicating that aerosols of one substance have a series of values of ρ_e^I and ρ_e^{III}, because aerosols have a wide size distribution. For example, particles with a ρ of 1.80 g/cm^3 and χ of 2.50 obtain ρ_e^I and ρ_e^{III} values of 0.43 g/cm^3 and 0.45 g/cm^3 at 40 nm, and of 0.22 g/cm^3 and 0.36 g/cm^3 at 550 nm, respectively. A series of values makes the physical quantities of ρ_e^I and ρ_e^{III} undistinguishable and blurs their physical meaning, which is totally inconsistent with the values of density.

3.3. The Independent Relationship between ρ_e^{II} and Particle Size

Figure 4 presents the ρ_e^{II} of Y and Z particles, showing that ρ_e^{II} only has one value in the entire range of sizes and that it is independent of particle size. This independent tendency is consistent with the characteristics of ρ. Therefore, it is more reasonable to use ρ_e^{II} as the alternative measure of density. The relationship between ρ_e and size is generally used to indicate the change in morphology and/or the transformation of the chemical compositions of particles. According to the new understanding of the relationship between the three effective densities and particle size from this study, Table 2 presents the relationship between the trends of effective density with size, and that of χ and ρ with size.

When ρ_e^I and ρ_e^{III} decrease with the increasing size of aspherical particles, they may be determined by the increase or invariability of χ for particles with a fixed ρ, and the decrease or the invariability of ρ for particles with a fixed χ. Even for the same physical quantity (e.g., χ, ρ), the change could result in the same trend of ρ_e^I and ρ_e^{III} with the particle size. In addition, it is worth noting that χ may change with particle size irregularly, [31] which will render the relationship of ρ_e^I and ρ_e^{III} with size more complicated. The above discussion suggests that the size-resolved ρ_e^I and ρ_e^{III} actually have no ability to indicate the relationship of χ and ρ with size. On the contrary, the increase, invariability, and decrease in ρ_e^{II} with the increasing size of aspherical particles specifically indicate the decrease in χ and/or the increase in ρ, the invariability of χ and/or ρ, and the increase in χ and/or the decrease in ρ, respectively. This comparison implies that ρ_e^{II} is a better indicator for the change in morphology and the transformation of the chemical compositions of particles. Therefore, it is recommended to apply ρ_e^{II} as an alternative measure of ρ in studies involving particle sizes in atmospheric science.
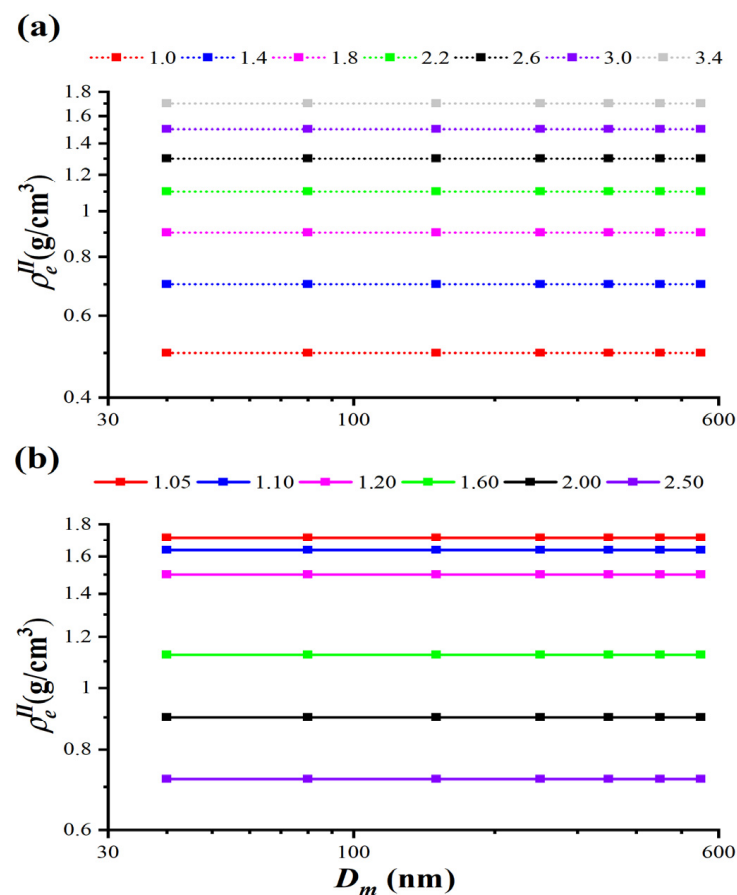
Figure 4. (**a**) The size-resolved ρ_e^{II} for the Y particles with ρ from 1.0 to 3.4 g/cm^3, which are represented by the change in line color from red to grey; (**b**) The size-resolved ρ_e^{II} for the Z particles with a χ from 1.05 to 2.50, which are represented by the change in line color from red to purple.

Table 2. The trends of ρ_e^I, ρ_e^{II}, and ρ_e^{III} with size of aspherical particles as χ (a) and ρ (b) change.

		The Trend of		
(a) Fixed value of ρ	χ	ρ_e^I	ρ_e^{II}	ρ_e^{III}
	Increasing	Decreasing	Decreasing	Decreasing
	Invariant	Decreasing	Invariant	Decreasing

Table 2. *Cont.*

	Decreasing	Invariant or increasing	Increasing	Invariant or increasing
(b) Fixed value of χ	ρ	$\rho_e{}^I$	$\rho_e{}^{II}$	$\rho_e{}^{III}$
	Increasing	Invariant or increasing	Increasing	Invariant or increasing
	Invariant	Decreasing	Invariant	Decreasing
	Decreasing	Decreasing	Decreasing	Decreasing

4. Conclusions

This study forms a comprehensive theoretical analysis for the three definitions of effective density. $\rho_e{}^{II}$ is found to be independent of particle size, while $\rho_e{}^I$ and $\rho_e{}^{III}$ decrease as the size of aspherical particles increases; these are determined by χ and $C_c(D_{ve})/C_c(D_m)$, but not ρ, which suggests that the relationship between size and the definitions of $\rho_e{}^I$ and $\rho_e{}^{III}$ gives little indication of the size-resolved physicochemical properties of the particle. Compared to $\rho_e{}^I$ and $\rho_e{}^{III}$, the values of $\rho_e{}^{II}$ are better for indicating the change in morphology and the transformation of chemical compositions; thus, the definition of $\rho_e{}^{II}$ is recommended as a more proper alternative measure of ρ in studies involving particle sizes in atmospheric science. These results lay a sound theoretical foundation for the three effective densities, which will help with their accurate application in the future studies.

Author Contributions: L.P. designed the research, performed the theoretical analysis, and wrote the manuscript. All co-authors discussed the results and commented on the manuscript. All authors have read and agreed to the published version of the manuscript.

Institutional Review Board Statement: Not applicable.

Informed Consent Statement: Not applicable.

Data Availability Statement: The datasets generated and analyzed during the current study are not publicly available but are available from the corresponding author on reasonable request.

Conflicts of Interest: The authors declare that they have no conflicts of interest.

Appendix A

Table A1. Introductions of the diameters used in this paper.

Symbol	Definition	Derivation	Example of Measurement Instrument
D_a	Aerodynamic diameter is defined as the diameter of a sphere with standard density that settles at the same terminal velocity as the particle of interest.	$D_a = D_{ve}\sqrt{\dfrac{\rho_p C_c(D_{ve})}{\chi \cdot \rho_0 \cdot C_c(D_a)}}$	Aerodynamic Aerosol Classifier (AAC)

Table A1. *Cont.*

D_{va}	In the free-molecular regime, the aerodynamic diameter is called the vacuum aerodynamic diameter.	$D_{va} = \frac{\rho_p}{\rho_0} \frac{D_{ve}}{\chi}$	Single-Particle Aerosol Mass Spectrometry (SPAMS)
D_m	Mobility diameter is defined as the diameter of a sphere with the same migration velocity in a constant electric field as the particle of interest.	$\frac{D_m}{C_c(D_m)} = \frac{D_{ve}}{C_c(D_{ve})}\chi$	Differential Mobility Analyzer (DMA)
D_{ve}	Volume-equivalent diameter is defined as the diameter of a spherical particle of the same volume as the particle under consideration.	$D_{ve} = \sqrt[3]{\frac{6m_p}{\pi \rho_p}}$	AAC-SPAMS

References

1. Buseck, P.R.; Posfai, M. Airborne minerals and related aerosol particles: Effects on climate and the environment. *Proc. Natl. Acad. Sci. USA* **1999**, *96*, 3372–3379. [CrossRef]
2. Poschl, U. Atmospheric aerosols: Composition, transformation, climate and health effects. *Angew. Chem. Int. Ed.* **2005**, *44*, 7520–7540. [CrossRef]
3. Katrib, Y.; Martin, S.T.; Rudich, Y.; Davidovits, P.; Jayne, J.T.; Worsnop, D.R. Density changes of aerosol particles as a result of chemical reaction. *Atmos. Chem. Phys.* **2005**, *5*, 275–291. [CrossRef]
4. Sumlin, B.J.; Oxford, C.R.; Seo, B.; Pattison, R.R.; Williams, B.J.; Chakrabarty, R.K. Density and Homogeneous Internal Composition of Primary Brown Carbon Aerosol. *Environ. Sci. Technol.* **2018**, *52*, 3982–3989. [CrossRef]
5. Nosko, O.; Olofsson, U. Effective density of airborne wear particles from car brake materials. *J. Aerosol Sci.* **2017**, *107*, 94–106. [CrossRef]
6. Guo, S.; Hu, M.; Zamora, M.L.; Peng, J.; Shang, D.; Zheng, J.; Du, Z.; Wu, Z.; Shao, M.; Zeng, L.; et al. Elucidating severe urban haze formation in China. *Proc. Natl. Acad. Sci. USA* **2014**, *111*, 17373–17378. [CrossRef]
7. Yin, Z.; Ye, X.; Jiang, S.; Tao, Y.; Shi, Y.; Yang, X.; Chen, J. Size-resolved effective density of urban aerosols in Shanghai. *Atmos. Environ.* **2015**, *100*, 133–140. [CrossRef]
8. Liu, Z.; Hu, B.; Ji, D.; Wang, Y.; Wang, M.; Wang, Y. Diurnal and seasonal variation of the PM2.5 apparent particle density in Beijing, China. *Atmos. Environ.* **2015**, *120*, 328–338. [CrossRef]
9. Yon, J.; Bescond, A.; Ouf, F.X. A simple semi-empirical model for effective density measurements of fractal aggregates. *J. Aerosol Sci.* **2015**, *87*, 28–37. [CrossRef]
10. DeCarlo, P.F.; Slowik, J.G.; Worsnop, D.R.; Davidovits, P.; Jimenez, J.L. Particle morphology and density characterization by combined mobility and aerodynamic diameter measurements. Part 1: Theory. *Aerosol Sci. Technol.* **2004**, *38*, 1185–1205. [CrossRef]
11. Hand, J.L.; Kreidenweis, S.M. A new method for retrieving particle refractive index and effective density from aerosol size distribution data. *Aerosol Sci. Technol.* **2002**, *36*, 1012–1026. [CrossRef]
12. Schneider, J.; Weimer, S.; Drewnick, F.; Borrmann, S.; Helas, G.; Gwaze, P.; Schmid, O.; Andreae, M.O.; Kirchner, U. Mass spectrometric analysis and aerodynamic properties of various types of combustion-related aerosol particles. *Int. J. Mass Spectrom.* **2006**, *258*, 37–49. [CrossRef]
13. Peng, L.; Li, Z.; Zhang, G.; Bi, X.; Hu, W.; Tang, M.; Wang, X.; Peng, P.; Sheng, G. A review of measurement techniques for aerosol effective density. *Sci. Total Environ.* **2021**, *778*, 146248. [CrossRef]
14. Schnitzler, E.G.; Dutt, A.; Charbonneau, A.M.; Olfert, J.S.; Jaeger, W. Soot Aggregate Restructuring Due to Coatings of Secondary Organic Aerosol Derived from Aromatic Precursors. *Environ. Sci. Technol.* **2014**, *48*, 14309–14316. [CrossRef]
15. Wu, Y.F.; Xia, Y.J.; Huang, R.J.; Deng, Z.Z.; Tian, P.; Xia, X.G.; Zhang, R.J. A study of the morphology and effective density of externally mixed black carbon aerosols in ambient air using a size-resolved single-particle soot photometer (SP2). *Atmos. Meas. Tech.* **2019**, *12*, 4347–4359. [CrossRef]
16. Spencer, M.T.; Prather, K.A. Using ATOFMS to determine OC/EC mass fractions in particles. *Aerosol Sci. Technol.* **2006**, *40*, 585–594. [CrossRef]
17. Bahreini, R.; Keywood, M.D.; Ng, N.L.; Varutbangkul, V.; Gao, S.; Flagan, R.C.; Seinfeld, J.H.; Worsnop, D.R.; Jimenez, J.L. Measurements of Secondary Organic Aerosol from Oxidation of Cycloalkenes, Terpenes, and m-Xylene Using an Aerodyne Aerosol Mass Spectrometer. *Environ. Sci. Technol.* **2005**, *39*, 5674–5688. [CrossRef]
18. Spencer, M.T.; Shields, L.G.; Prather, K.A. Simultaneous measurement of the effective density and chemical composition of ambient aerosol particles. *Environ. Sci. Technol.* **2007**, *41*, 1303–1309. [CrossRef]
19. Zhai, J.H.; Lu, X.H.; Li, L.; Zhang, Q.; Zhang, C.; Chen, H.; Yang, X.; Chen, J.M. Size-resolved chemical composition, effective density, and optical properties of biomass burning particles. *Atmos. Chem. Phys.* **2017**, *17*, 7481–7493. [CrossRef]

20. Murphy, S.M.; Agrawal, H.; Sorooshian, A.; Padro, L.T.; Gates, H.; Hersey, S.; Welch, W.A.; Jung, H.; Miller, J.W.; Cocker, D.R.; et al. Comprehensive Simultaneous Shipboard and Airborne Characterization of Exhaust from a Modern Container Ship at Sea. *Environ. Sci. Technol.* **2009**, *43*, 4626–4640. [CrossRef]

21. Peng, L.; Li, L.; Zhang, G.; Du, X.; Wang, X.; Peng, P.a.; Sheng, G.; Bi, X. Technical note: Measurement of chemically resolved volume equivalent diameter and effective density of particles by AAC-SPAMS. *Atmos. Chem. Phys.* **2021**, *21*, 5605–5613. [CrossRef]

22. Park, K.; Cao, F.; Kittelson, D.B.; McMurry, P.H. Relationship between particle mass and mobility for diesel exhaust particles. *Env. Sci. Technol.* **2003**, *37*, 577–583. [CrossRef]

23. Deye, G.J.; Kulkarni, P.; Ku, B.K. Morphological characterization of carbon nanofiber aerosol using tandem mobility and aerodynamic size measurements. *J. Nanopart. Res.* **2012**, *14*, 1112. [CrossRef]

24. Momenimovahed, A.; Olfert, J.S. Effective Density and Volatility of Particles Emitted from Gasoline Direct Injection Vehicles and Implications for Particle Mass Measurement. *Aerosol Sci. Technol.* **2015**, *49*, 1051–1062. [CrossRef]

25. Alexander, J.M.; Bell, D.M.; Imre, D.; Kleiber, P.D.; Grassian, V.H.; Zelenyuk, A. Measurement of size-dependent dynamic shape factors of quartz particles in two flow regimes. *Aerosol Sci. Technol.* **2016**, *50*, 870–879. [CrossRef]

26. Afroughi, M.J.; Falahati, F.; Kostiuk, L.W.; Olfert, J.S. Properties of carbon black produced by the thermal decomposition of methane in the products of premixed flames. *J. Aerosol Sci.* **2019**, *131*, 13–27. [CrossRef]

27. Olfert, J.; Rogak, S. Universal relations between soot effective density and primary particle size for common combustion sources. *Aerosol Sci. Technol.* **2019**, *53*, 485–492. [CrossRef]

28. Alfarra, M.R.; Paulsen, D.; Gysel, M.; Garforth, A.A.; Dommen, J.; Prevot, A.S.H.; Worsnop, D.R.; Baltensperger, U.; Coe, H. A mass spectrometric study of secondary organic aerosols formed from the photooxidation of anthropogenic and biogenic precursors in a reaction chamber. *Atmos. Chem. Phys.* **2006**, *6*, 5279–5293. [CrossRef]

29. Hu, M.; Peng, J.F.; Sun, K.; Yue, D.L.; Guo, S.; Wiedensohler, A.; Wu, Z.J. Estimation of size-resolved ambient particle density based on the measurement of aerosol number, mass, and chemical size distributions in the winter in Beijing. *Environ. Sci. Technol.* **2012**, *46*, 9941–9947. [CrossRef]

30. Rissler, J.; Nordin, E.Z.; Eriksson, A.C.; Nilsson, P.T.; Frosch, M.; Sporre, M.K.; Wierzbicka, A.; Svenningsson, B.; Londahl, J.; Messing, M.E.; et al. Effective Density and Mixing State of Aerosol Particles in a Near-Traffic Urban Environment. *Environ. Sci. Technol.* **2014**, *48*, 6300–6308. [CrossRef]

31. Zieger, P.; Vaisanen, O.; Corbin, J.C.; Partridge, D.G.; Bastelberger, S.; Mousavi-Fard, M.; Rosati, B.; Gysel, M.; Krieger, U.K.; Leck, C.; et al. Revising the hygroscopicity of inorganic sea salt particles. *Nat. Commun.* **2017**, *8*, 15883. [CrossRef]

32. Khlystov, A.; Stanier, C.; Pandis, S.N. An algorithm for combining electrical mobility and aerodynamic size distributions data when measuring ambient aerosol. *Aerosol Sci. Technol.* **2004**, *38*, 229–238. [CrossRef]

33. Beddows, D.C.S.; Dall'osto, M.; Harrison, R.M. An Enhanced Procedure for the Merging of Atmospheric Particle Size Distribution Data Measured Using Electrical Mobility and Time-of-Flight Analysers. *Aerosol Sci. Technol.* **2010**, *44*, 930–938. [CrossRef]

34. Kassianov, E.; Barnard, J.; Pekour, M.; Berg, L.K.; Shilling, J.; Flynn, C.; Mei, F.; Jefferson, A. Simultaneous retrieval of effective refractive index and density from size distribution and light-scattering data: Weakly absorbing aerosol. *Atmos. Meas. Tech.* **2014**, *7*, 3247–3261. [CrossRef]

35. Zhao, S.P.; Yu, Y.; Yin, D.Y.; He, J.J. Effective Density of Submicron Aerosol Particles in a Typical Valley City, Western China. *Aerosol Air Qual. Res.* **2017**, *17*, 1–13. [CrossRef]

36. Han, C.; Li, S.M.; Liu, P.; Lee, P. Size Dependence of the Physical Characteristics of Particles Containing Refractory Black Carbon in Diesel Vehicle Exhaust. *Environ. Sci. Technol.* **2019**, *53*, 137–145. [CrossRef]

37. Rissler, J.; Messing, M.E.; Malik, A.I.; Nilsson, P.T.; Nordin, E.Z.; Bohgard, M.; Sanati, M.; Pagels, J.H. Effective Density Characterization of Soot Agglomerates from Various Sources and Comparison to Aggregation Theory. *Aerosol Sci. Technol.* **2013**, *47*, 792–805. [CrossRef]

38. Dastanpour, R.; Momenimovahed, A.; Thomson, K.; Olfert, J.; Rogak, S. Variation of the optical properties of soot as a function of particle mass. *Carbon* **2017**, *124*, 201–211. [CrossRef]

39. Kiselev, A.; Wennrich, C.; Stratmann, F.; Wex, H.; Henning, S.; Mentel, T.F.; Kiendler-Scharr, A.; Schneider, J.; Walter, S.; Lieberwirth, I. Morphological characterization of soot aerosol particles during LACIS Experiment in November (LExNo). *J. Geophys. Res. Atmos.* **2010**, *115*, 11204. [CrossRef]

40. Leskinen, J.; Ihalainen, M.; Torvela, T.; Kortelainen, M.; Lamberg, H.; Tiitta, P.; Jakobi, G.; Grigonyte, J.; Joutsensaari, J.; Sippula, O.; et al. Effective Density and Morphology of Particles Emitted from Small-Scale Combustion of Various Wood Fuels. *Environ. Sci. Technol.* **2014**, *48*, 13298–13306. [CrossRef]

41. Dinar, E.; Mentel, T.F.; Rudich, Y. The density of humic acids and humic like substances (HULIS) from fresh and aged wood burning and pollution aerosol particles. *Atmos. Chem. Phys.* **2006**, *6*, 5213–5224. [CrossRef]

42. Qiu, C.; Khalizov, A.F.; Zhang, R. Soot Aging from OH-Initiated Oxidation of Toluene. *Environ. Sci. Technol.* **2012**, *46*, 9464–9472. [CrossRef] [PubMed]

43. Khalizov, A.F.; Lin, Y.; Qiu, C.; Guo, S.; Collins, D.; Zhang, R. Role of OH-Initiated Oxidation of Isoprene in Aging of Combustion Soot. *Environ. Sci. Technol.* **2013**, *47*, 2254–2263. [CrossRef] [PubMed]